# Wind-Optimal Cruise Airspeed for a Multirotor Aircraft in Urban Air Mobility

Priyank Pradeep \*

Universities Space Research Association, NASA Ames Research Center, Moffett Field, CA, 94035, USA.

Todd A. Lauderdale <sup>†</sup>, and Heinz Erzberger <sup>‡</sup> *NASA Ames Research Center, Moffett Field, CA, 94035, USA.* 

Gano B. Chatterji §

Crown Consulting Inc, NASA Ames Research Center, Moffett Field, CA, 94035, USA.

This paper first investigates the effect of wind on the wind-optimal (minimum-energy) cruise airspeed for a NASA-proposed conceptual multirotor aircraft for the urban air mobility environment. Next, energy consumption and flight duration results are compared for flying at the wind-optimal airspeed and best-range airspeed on a great-circle cruise segment under different wind conditions. Finally, the difference in energy consumption when flying to meet the assigned required time of arrival based on actual wind conditions vs. predicted wind conditions are examined and compared for the two airspeed modes (wind-optimal and best-range) for different values of wind magnitude uncertainty. The results show operational benefits of flying at the wind-optimal cruise airspeed compared to the best-range airspeed, especially under strong headwind conditions from both an energy consumption and flight duration perspective. The results also show that flying at wind-optimal airspeed under wind magnitude uncertainty has lower variability and higher predictability of energy consumption than flying at best-range airspeed.

#### I. Nomenclature

= Latitude of the aircraft λ Longitude of the aircraft τ h = Altitude above mean sea level of the aircraft = Mass of the aircraft m VTrue airspeed of the aircraft  $V_{GS}$ Groundspeed of the aircraft Aerodynamic flight path angle of the aircraft γ Heading angle of the aircraft ψ Course angle of the aircraft X Parasite drag on the aircraft D T= Net thrust Number of rotors installed on the aircraft nAngle-of-attack of air-stream relative to rotor tip-path-plane  $\alpha$  $\theta$ Rotor tip-path-plane pitch angle Rotor tip-path-plane roll angle φ Induced power factor К Rotational speed of the rotor blades Thrust weighted solidity ratio  $C_{\mathrm{d\ mean}}$ = Mean blade drag coefficient

<sup>\*</sup>Aerospace Engineer, Universities Space Research Association, NASA Ames Research Center, AIAA Senior Member.

<sup>&</sup>lt;sup>†</sup> Aerospace Engineer, Aviation Systems Division, NASA Ames Research Center.

<sup>&</sup>lt;sup>‡</sup>Ames Associate, Aviation Systems Division, NASA Ames Research Center, AIAA Fellow.

<sup>§</sup> Senior Scientist and Lead, Crown Consulting Inc., NASA Ames Research Center, AIAA Associate Fellow.

 $A_{\text{rotor}}$  = Rotor disk area R = Radius of the rotor

 $v_h$  = Rotor induced velocity in hover

 $v_i$  = Rotor induced velocity during forward flight

 $T_{\text{rotor}}$  = Thrust produced by an isolated rotor

 $C_{\rm T}$  = Rotor thrust coefficient

 $I_i$  = Moment of inertia of the  $i^{th}$  rotor  $P_{\text{max}}$  = Total maximum deliverable power

 $P_{\text{req}}$  = Instantaneous power required in forward flight

 $P_{\text{battery}}$  = Instantaneous power supplied by the onboard lithium-ion polymer battery pack

 $\rho$  = Density of air

 $R_{\text{Earth}}$  = Radius of the Earth assuming spherical model

 $W_e$  = East component of wind velocity  $W_n$  = North component of wind velocity DEP = Distributed electric propulsion EVTOL = Electric vertical takeoff and landing

Li-Po = Lithium-ion polymer battery RTA = Required time of arrival UAM = Urban air mobility

UTM = Unmanned aircraft system traffic management

 $V_{\rm MO}$  = Maximum operating limit airspeed

# **II. Airspeed Definition**

The definition of airspeed terms used in this research are as follows:

- Max-Endurance Airspeed: The airspeed at which power required  $(P_{req})$  by the multirotor aircraft is minimum [1].
- Best-Range Airspeed: The energy-optimal (minimum-energy) airspeed for a fixed range in the absence of wind. The best-range airspeed is also the airspeed at which the ratio of power required (P<sub>req</sub>) and true airspeed (V) is minimum [1]; therefore, the range is maximized for given onboard battery capacity in the absence of wind. The best-range airspeed data is typically published in the aircraft/helicopter performance manual of an aircraft/helicopter type.
- Wind-Optimal Airspeed: The energy-optimal (minimum-energy) airspeed for fixed range considering wind conditions [2]. Therefore, the wind-optimal airspeed is best-range airspeed corrected for wind conditions for a fixed range.

# **III. Introduction**

Road traffic congestion adversely impacts passenger transportation, cargo delivery, and emergency services in major metropolitan areas. The envisioned concept of urban air mobility (UAM) involves a network of electric vertical takeoff and landing (eVTOL) aircraft that can enable rapid and reliable transportation in metropolitan areas by utilizing three-dimensional (3D) airspace efficiently [3–5].

Recently, technological advances have made it possible to build and flight test eVTOL aircraft [4–6]. Several companies, for example, Airbus A<sup>3</sup>, Aurora Flight Sciences, EHang, Joby Aviation, Wisk (Kitty Hawk), Leonardo, Lilium, Terrafugia, and Volocopter, are pursuing different design approaches to make eVTOLs a reality [5]. Despite various designs, they all have distributed electric propulsion (DEP) systems in common [4]. However, the low specific energy of current lithium-ion polymer (Li-Po) battery technology used in DEP imposes constraints on such aircraft's flight endurance. Therefore, to enable autonomous urban air mobility operations using electric aircraft, one of the critical steps from a safety perspective is to accurately and periodically predict whether the current state of the onboard Li-Po battery pack is sufficient to support the flight mission under given operational and environmental conditions with an adequate safety margin [7]. On the other hand, from an efficiency perspective, an essential step is to understand the most energy-efficient flight profile (cruise airspeed, cruise altitude, and climb and descent profiles). In research [4, 8], energy-efficient climb profile, descent profile, cruise altitude, and best-range airspeed have been studied for multirotor aircraft. In general, multirotor aircraft are relatively low-cruise-speed aircraft than winged eVTOL aircraft [9]; therefore, atmospheric winds play a more significant role in their trajectories. In research [10], operational benefits

of flying wind-optimal lateral trajectories have been explored for multirotor aircraft. But, the research did not look at wind-optimal (minimum-energy) airspeed as a function of wind direction and magnitude. The operational benefits of flying wind-optimal airspeed have been studied for a helicopter (Sikorsky S-61N) [2], but not for multirotor aircraft for the UAM environment. As stated earlier, the wind-optimal airspeed is the energy-optimal (minimum-energy) airspeed for a given cruise segment and wind conditions. Therefore, this paper's primary contribution is to explore wind-optimal cruise airspeed and then quantify the operational benefits of using wind-optimal cruise airspeed.

The rest of the paper is organized as follows. In Section IV, an optimal control problem is formulated to quantify the effect of wind on the wind-optimal (minimum-energy) cruise airspeed for a multirotor aircraft for the urban air mobility environment (range and altitude). In Section V, first, wind-optimal cruise airspeed is explored for a NASA-proposed conceptual multirotor aircraft flight as a function of wind magnitude and direction. Next, energy consumption and flight duration results are compared for a variety of trajectory types in the cruise phase under different wind conditions. In Section VI, the operational benefits of flying the wind-optimal cruise airspeed under wind magnitude uncertainty are examined. In Section VII, the main findings from this research study are summarized.

# IV. Optimal Control Problem Formulation

# A. Flight Dynamics, Flight Kinematics, Thrust and Drag Models

In this research, a quadrotor eVTOL aircraft concept proposed by Silva et al. [9], as shown in Figure 1a, is used to study operational benefits of flying wind-optimal cruise airspeed. The quasi-steady lateral flight dynamics and kinematics model used in this research for the trajectory optimization in cruise phase is from [4, 8, 10–13]:

$$\frac{dV}{dt} = \frac{T\cos\phi\sin\theta - D}{m} \tag{1}$$

$$\frac{d\psi}{dt} = \frac{T\sin\phi}{mV} \tag{2}$$

$$\frac{d\lambda}{dt} = \frac{V\cos\psi + W_n}{(R_{\text{Earth}} + h)} = \frac{V_{GS}\cos\chi}{(R_{\text{Earth}} + h)}$$
(3)

$$\frac{d\tau}{dt} = \frac{V\sin\psi + W_e}{(R_{\text{Earth}} + h)\cos\lambda} = \frac{V_{GS}\sin\chi}{(R_{\text{Earth}} + h)\cos\lambda}$$
(4)

where m is the mass of the multirotor aircraft, D is the parasite drag,  $V_{GS}$  is the groundspeed,  $\chi$  is the course, h is the altitude above mean sea level,  $R_{\text{Earth}}$  is the mean radius of the Earth, and  $W_e$  and  $W_n$  are the components of the wind in east and north directions, respectively. The four lateral states of the model are [4, 8, 10-13]:

$$X = [\lambda \tau V \psi]^T \tag{5}$$

where  $\lambda$  is the latitude,  $\tau$  is the longitude, V is the true airspeed and  $\psi$  is the heading angle w.r.t north as shown in Figures 1b, 1c and 1d [8, 10]. In this research, the true airspeed is assumed to have only a lateral component, i.e., no vertical component. The three control variables related to the flight dynamics model are [4, 8, 10–12]:

$$C = [T \theta \phi]^T \tag{6}$$

where T is the net thrust,  $\theta$  is the rotor tip-path-plane pitch angle and  $\phi$  is the rotor tip-path-plane roll (bank) angle as shown in Figures 1c and 1d.

The net thrust (T) for the multirotor aircraft, assuming that the rotors have negligible interference with each other and produce the same amount of thrust is given by [10]:

$$T = 4T_{\text{rotor}} \tag{7}$$

where  $T_{\text{rotor}}$  is the thrust produced by a single rotor.

The parasite drag (D) on the multirotor aircraft is calculated as follows [9, 10]:

$$D = 1.1984q (8)$$

where q is the dynamic pressure  $(N/m^2)$ .

#### **B.** Power Required

The instantaneous power required in forward flight is equal to the sum of the induced power, parasite power, climb power and profile power as follows [1, 7, 8, 10]:

$$P_{\text{required}} = P_{\text{induced}} + P_{\text{parasite}} + P_{\text{climb}} + P_{\text{profile}}$$
(9)

The power required by the multirotor aircraft in forward flight is as follows [1, 8, 10]

$$P_{\text{required}} = \kappa \sum_{n=1}^{4} (T_{\text{rotor}} v_i)_n + TV \sin \alpha + \frac{\rho A_{\text{rotor}} (\omega R)^3 \sigma C_{d \ mean} F_P}{8}$$
 (10)

where  $v_i$  is the induced velocity,  $\kappa$  is the induced power correction factor,  $\alpha$  is the angle of attack between the air-stream and the rotor disk (tip-path-plane),  $C_{\rm d\,mean}$  is the mean blade drag coefficient,  $\sigma$  is the thrust weighted solidity ratio and  $F_{\rm P}$  is the function that accounts for the increase of the blade section velocity with rotor edgewise and axial speed [1, 7]. The induced velocity ( $v_i$ ) is numerically computed as described in [10]. The  $C_{\rm d\,mean}$  and  $\kappa$  are computed as a function of the advance ratio ( $\mu$ ) as defined in [8].

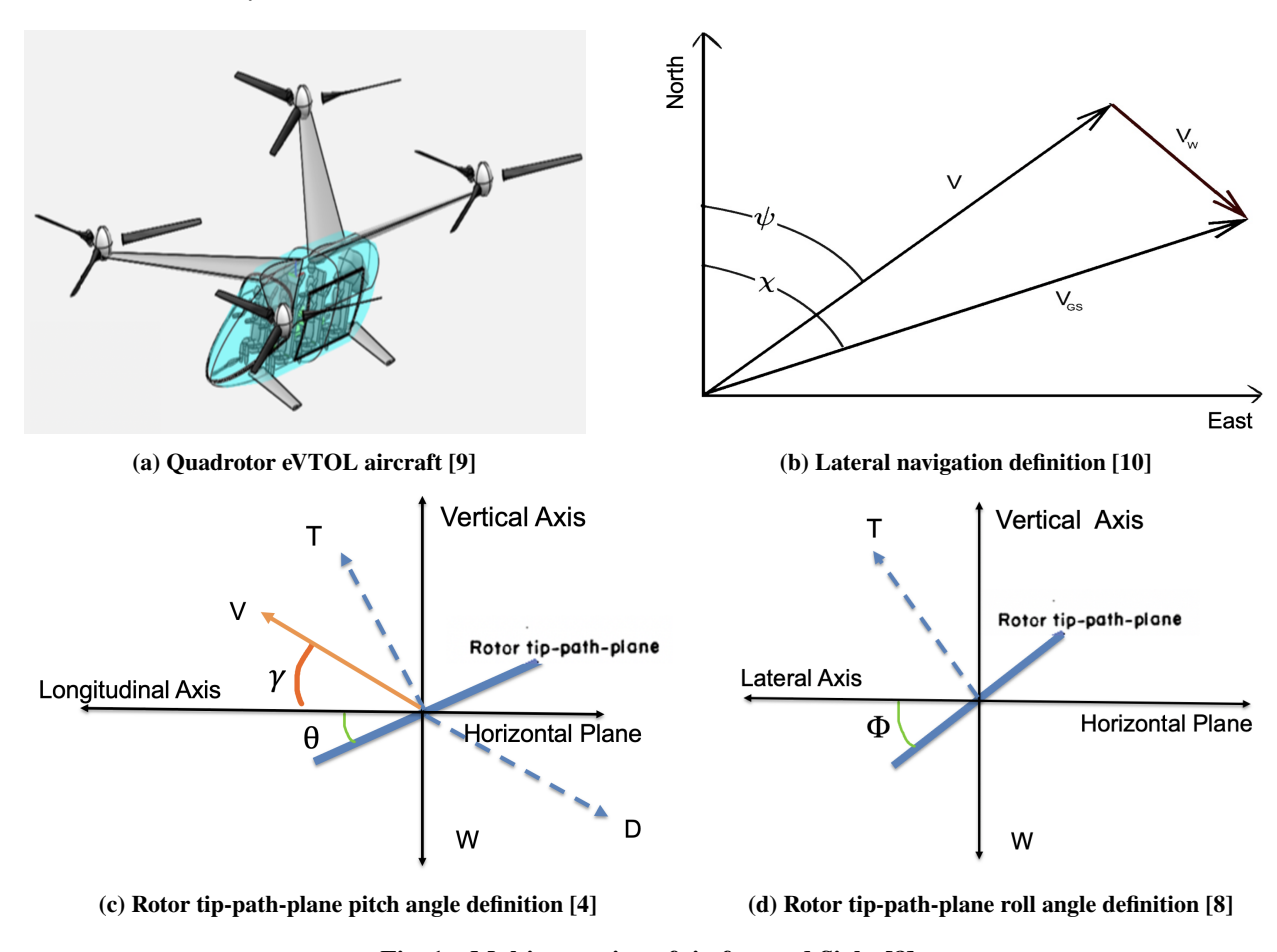


Fig. 1 Multirotor aircraft in forward flight [8]

#### C. Performance Index

To compute energy consumption using the power required (Equation: 10), the performance index for the problem is constructed as follows:

$$J = \int_{t_0}^{t_f} (P_{\text{required}}) dt = \int_{t_0}^{t_f} (\kappa \sum_{n=1}^{4} (T_{\text{rotor}} v_i)_n + TV \sin \alpha + \frac{\rho A_{\text{rotor}} (\Omega R)^3 \sigma C_{d \ mean} F_P}{8}) dt$$
(11)

where  $t_0$  is the initial flight time at the top-of-climb (TOC) and  $t_f$  is the final flight time to reach the top-of-descent (TOD).

#### D. Path Constraints of the Problem

For a level flight (cruise) in the presence of zero vertical wind, the net vertical force on the multirotor aircraft is zero; therefore, the following path constraint is imposed on the problem [10]:

$$T\cos\phi\cos\theta = mg\tag{12}$$

where m is the mass of the multirotor aircraft and g is the acceleration due to the gravity. For a cruise at constant airspeed, upper and lower bounds on the true airspeed (V) is set to the same value in the optimal control solver.

The path constraint for the great-circle trajectory between the two waypoints is given by [10]:

$$(V\sin\psi + W_e)(\sin\lambda_2\cos\lambda_1 - \sin\lambda_1\cos\lambda_2\cos(\tau_2 - \tau_1)) - (V\cos\psi + W_n)(\sin(\tau_2 - \tau_1)\cos\lambda_2) = 0$$
 (13)

The instantaneous power required (Equation: 10) is bounded by the total maximum available power to the four rotors in kW [7, 9]:

$$P_{\text{required}} \le 494.25 \tag{14}$$

#### E. Performance Data

The performance data of the NASA-proposed conceptual multirotor aircraft used in this research is per [8, 9]. The thrust coefficient ( $C_T$ ) is approximated as a constant assuming that a collective pitch control mechanism is used for the rotor thrust magnitude control [7].

# V. Case Studies and Results

#### A. Parametric Approach to Compute Wind-Optimal Cruise Airspeed using Optimal Control Framework

Table 1 Great-circle cruise segments

Initial Waypoint (lat, lon)	Final Waypoint (lat, lon)	Cruise Segment (nm)
(41.204, -74.176)	(40.704, -74.176)	30 nm
(41.204, -74.176)	(39.538, -74.176)	100 nm

In this research, great-circle trajectories are generated using the state equations (Equations: 1 - 4) and great-circle navigation law (Equation: 13) that employs thrust (T), rotor tip-path-plane pitch ( $\theta$ ) and rotor tip-path-plane bank ( $\phi$ ) angles as controls. The equations of motion are integrated forward in time using the controls needed for following the desired lateral path (great-circle) in the cruise phase [14]. The wind-optimal cruise airspeed for a given set of conditions is computed using the parametric approach as shown in Figure 2. For a given initial waypoint (top of climb) and final waypoint (top of descent) at cruise altitude, wind conditions, and path constraints, the cruise airspeed is varied from 20 m/s (38.87 kts) to 60 m/s (116.63 kts) based on the max-endurance airspeed (30 m/s) to  $V_{\rm MO}$  (56 m/s) of the multirotor aircraft [9]. Finally, the wind-optimal (minimum-energy) cruise airspeed is chosen for the given set of conditions as the one with the least amount of energy consumption as shown in Figure 2.

The wind-optimal cruise airspeeds are computed using a parametric approach (Figure 2) for different cruise altitudes: [500 m (1640 ft), 1000 m (3280 ft), 2000 m (6561 ft), 3000 m (9842 ft)] [9], wind magnitudes: [0 kts, 13 kts, 26 kts, 39 kts] [15], and wind directions: [headwind, tailwind, crosswind] based on flyable operating environment for the multirotor aircraft. Two different great-circle paths of lengths 30 nm and 100 nm (Table 1) are considered for the fixed range problem.

Traditionally, the best-range airspeed for an aircraft is computed under no-wind conditions using an analytical or numerical approach [16]. In research [8], the best-range airspeed for the NASA-proposed multirotor aircraft [9] is computed using a similar parametric approach as that for wind-optimal airspeed (shown in Figure 2), however, in the absence of wind. Therefore, wind-optimal airspeed is the best-range airspeed corrected for wind conditions.

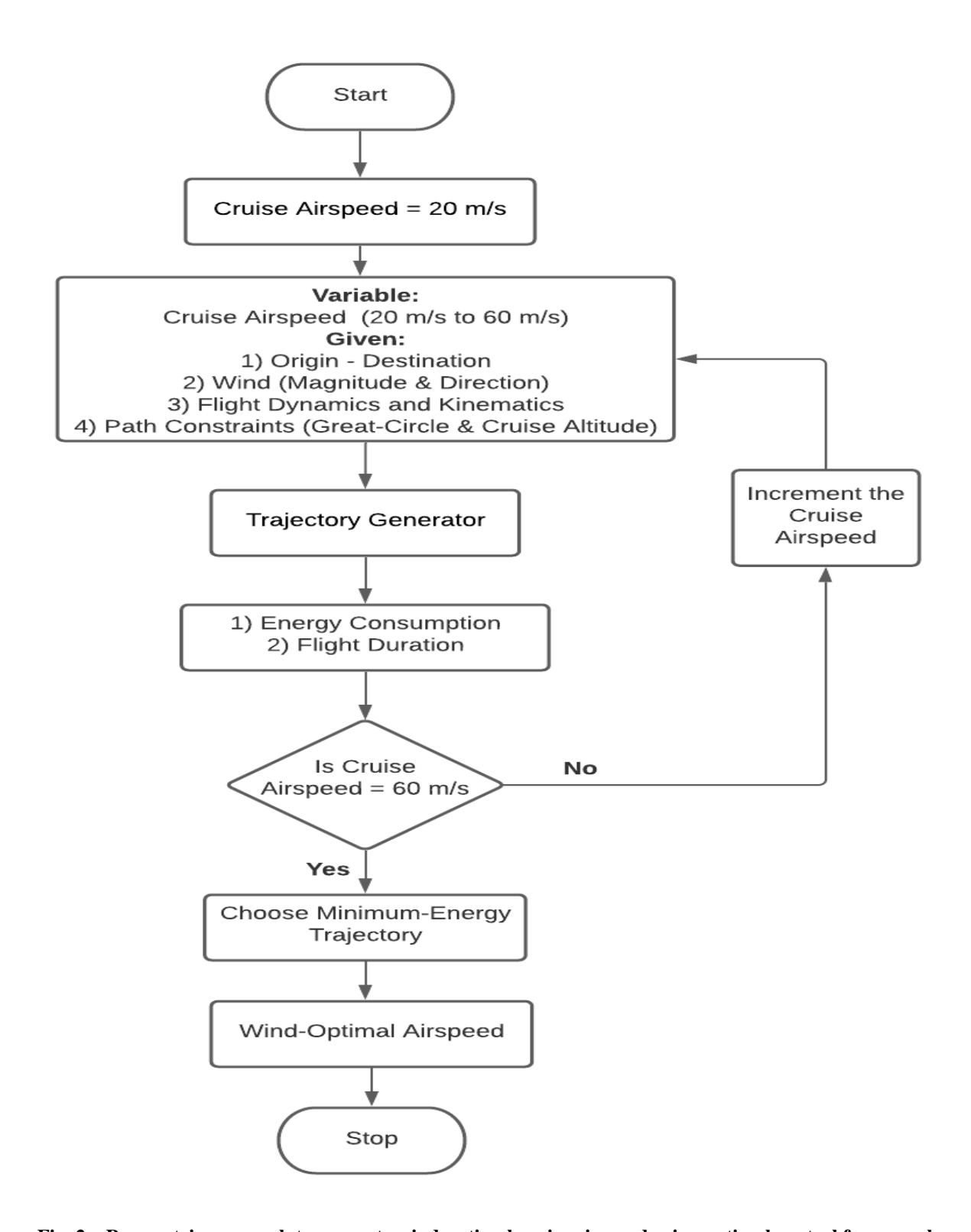


Fig. 2 Parametric approach to compute wind-optimal cruise airspeed using optimal control framework

#### **B.** Metrics to Measure Operational Benefits

Under given wind conditions, the energy savings (%) associated with flying a great-circle cruise segment at the wind-optimal airspeed compared to the best-range airspeed is computed as follows:

Energy Savings (%) = 
$$\frac{\text{Energy}_{\text{Best-Range}} - \text{Energy}_{\text{Wind-Optimal}}}{\text{Energy}_{\text{Best-Range}}} 100$$
 (15)

where Energy<sub>Best-Range</sub> and Energy<sub>Wind-Optimal</sub> are energy consumed flying a given great-circle cruise segment at the best-range airspeed and wind-optimal airspeed under similar wind conditions respectively.

The flight duration savings (%) associated with flying a great-circle cruise segment at the wind-optimal airspeed compared to the best-range airspeed is computed as follows:

Flight Duration Savings (%) = 
$$\frac{\text{Flight Duration}_{\text{Best-Range}} - \text{Flight Duration}_{\text{Wind-Optimal}}}{\text{Flight Duration}_{\text{Best-Range}}} 100 \tag{16}$$

where Flight Duration<sub>Best-Range</sub> and Flight Duration<sub>Wind-Optimal</sub> are flight duration flying a given great-circle cruise segment at the best-range airspeed and wind-optimal airspeed under similar wind conditions respectively.

#### C. Wind-Optimal Cruise Airspeed

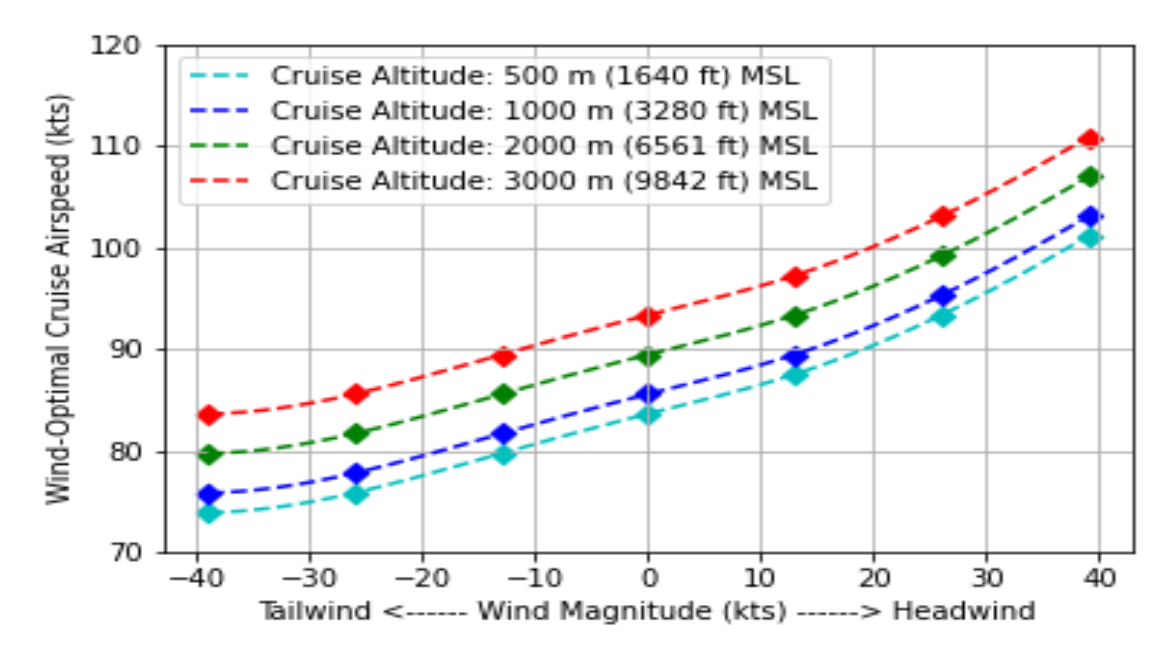


Fig. 3 Depiction of variation in wind-optimal cruise airspeed as a function of wind magnitude, wind direction, and cruise altitude for a NASA-proposed conceptual multirotor aircraft

## 1. Headwind and Tailwind Conditions

The wind-optimal cruise airspeeds are computed for different cruise altitudes: [500 m (1640 ft), 1000 m (3280 ft), 2000 m (6561 ft), 3000 m (9842 ft)] above mean sea level, wind magnitudes: [0 kts, 13 kts, 26 kts, 39 kts], and wind directions: [headwind, tailwind] as shown in Figure 3 using parametric approach as shown in Figure 2. The headwind is depicted as positive and the tailwind as negative in Figure 3 and Figure 6. Two great-circle cruise segments of length 30 nm and 100 nm are considered as shown in Table 1 for the computation of wind-optimal airspeeds. During the parametric study, the same wind-optimal (minimum-energy) cruise airspeed is observed for a given set of conditions (cruise altitude and wind) irrespective of the cruise segment length (30 nm or 100 nm).

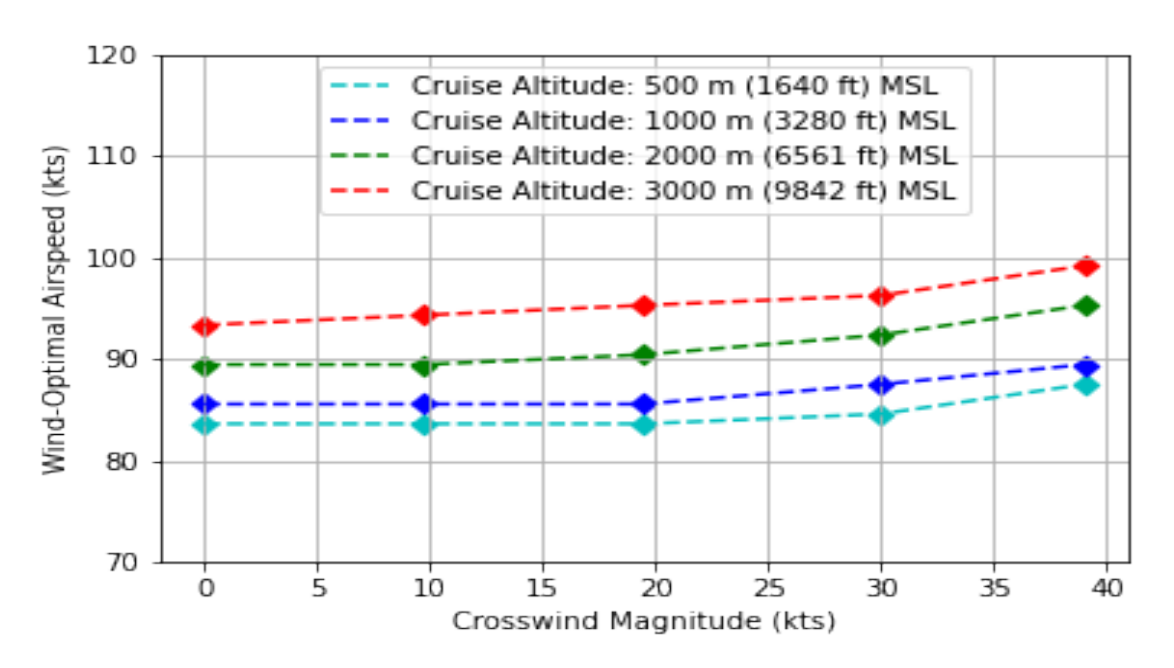


Fig. 4 Depiction of variation in wind-optimal cruise airspeed as a function of crosswind magnitude, and cruise altitude for a NASA-proposed conceptual multirotor aircraft

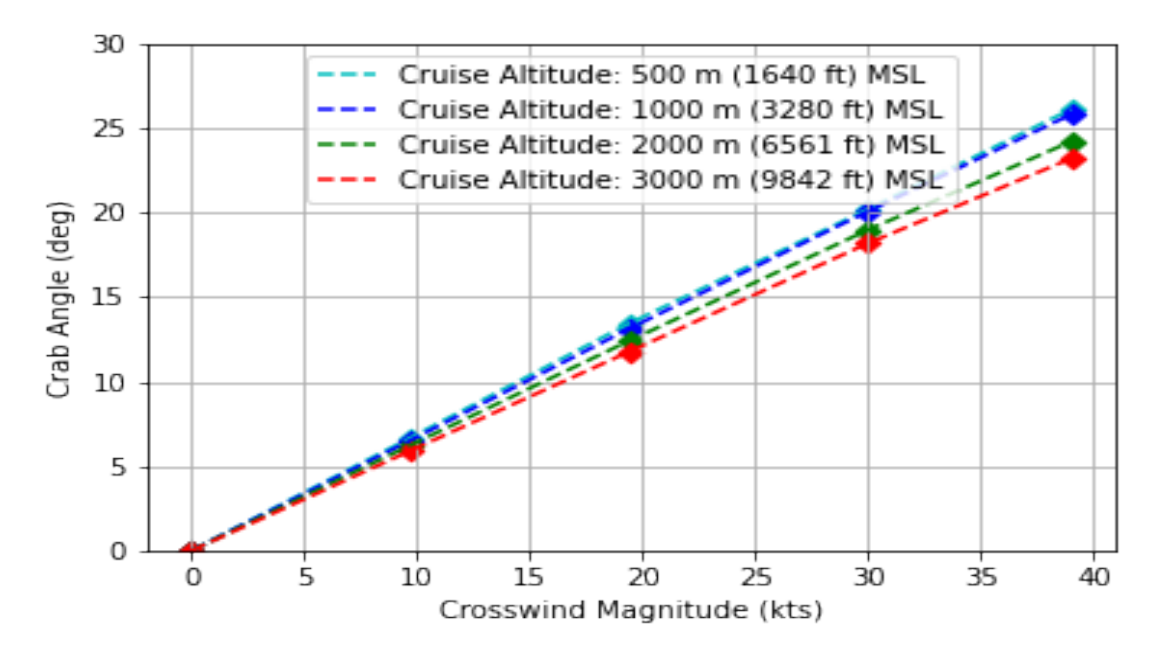


Fig. 5 Depiction of variation in crab angle as a function of crosswind magnitude, and cruise altitude for a NASA-proposed conceptual multirotor aircraft

Figure 3 shows that in the presence of the headwind or tailwind, the minimum-energy airspeed is different from the best-range airspeed, i.e., minimum-energy airspeed in the absence of wind. The wind-optimal cruise airspeed is faster than the best-range airspeed under headwind conditions and slower than the best-range airspeed under tailwind conditions. Also, the shift of the wind-optimal cruise airspeed from the best-range airspeed is a function of the wind magnitude, wind direction, and cruise altitude.

#### 2. Crosswind Conditions

The wind-optimal cruise airspeeds and crab angles computed for different cruise altitudes: [500 m (1640 ft), 1000 m (3280 ft), 2000 m (6561 ft), 3000 m (9842 ft)] above mean sea level, and crosswind magnitudes: [0 kts, 10 kts, 19.5 kts, 30 kts, 39 kts] are shown in Figure 4 and Figure 5. A great-circle cruise segment of length 30 nm is considered as shown in Table 1 for the computation of wind-optimal airspeeds and crab angles under different crosswind conditions.

Figure 4 shows that the shift of the wind-optimal cruise airspeed from the corresponding best-range airspeed is a function of the crosswind magnitude and cruise altitude. From Figure 4 it can also be seen that the impact of the crosswind on the minimum-energy (wind-optimal) airspeed is small compared to the effect of headwind of the same magnitude. The wind-optimal cruise airspeed is slightly faster than the corresponding best-range airspeed when the crosswind exceeds approximately 20 kts. However, Figure 5 shows crab angle required to fly on a great-circle cruise segment is a linear function of crosswind magnitude.

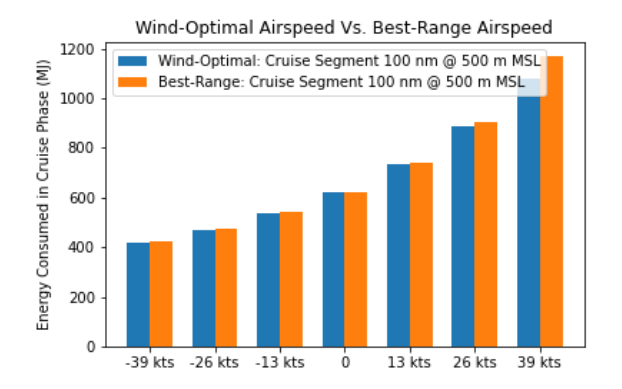
## D. Comparison of Operational Benefits Flying Wind-Optimal Vs Best-Range Cruise Airspeed

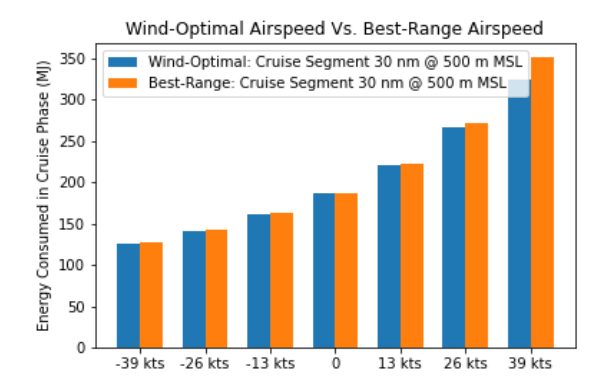
#### 1. Headwind and Tailwind Conditions

The Sub-figures in Figure 6 show the operational benefits of flying wind-optimal cruise airspeed compared to the best-range airspeed, from energy consumption and flight duration perspective. From Sub-figures 6a, 6b, 6c and 6d, it can be seen that (irrespective of the cruise segment length) flying at wind-optimal airspeed under tailwind or headwind conditions saves energy compared to flying at the best-range airspeed. For example, flying a great-circle cruise segment under 39 kts of constant headwind at wind-optimal airspeed can save energy between 6 to 7.5 % depending upon the cruise altitude compared to flying under the same conditions at the best-range airspeed. On the other hand, from a flight duration savings perspective, from Sub-figures 6e and 6f, it can be seen that flying under headwind conditions at wind-optimal airspeed reduces flight duration compared to flying at the best-range airspeed. However, flying under tailwind conditions at wind-optimal airspeed increases the flight duration compared to flying at the best-range airspeed. For example, flying a great-circle cruise segment under 39 kts of constant headwind at wind-optimal airspeed can reduce flight duration between 25 to 28 % depending on the cruise altitude as compared to flying under the same conditions at the best-range airspeed.

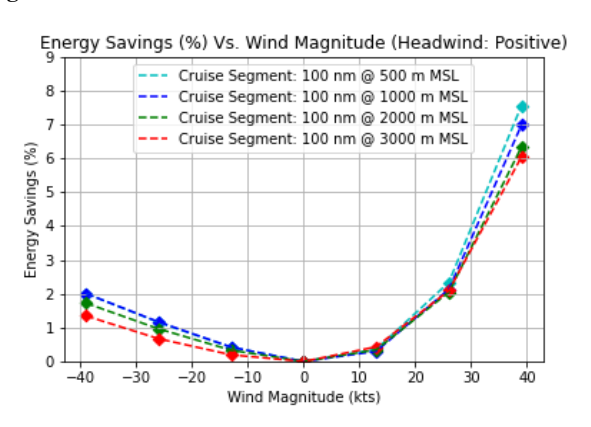
## 2. Crosswind Conditions

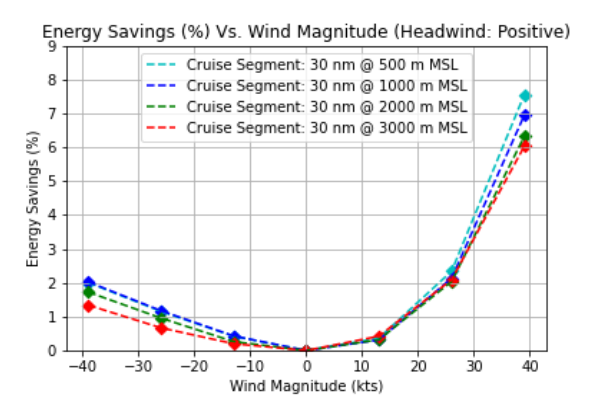
From Sub-figures 7a and 7b, it can be seen that flying at wind-optimal airspeed under crosswind conditions saves energy compared to flying at the best-range airspeed only when crosswind magnitude is greater than 20 kts. However, these values are small (0 to 0.75 %) compared to the advantage of flying wind-optimal airspeed under similar magnitude of headwind (0 to 7.5 %). For example, flying a great-circle cruise segment under 39 kts of constant headwind at wind-optimal airspeed can save energy between 0.5 to 0.75 % and flight duration between 3 to 6 % based on the cruise altitude compared to flying under the same conditions at the best-range airspeed.



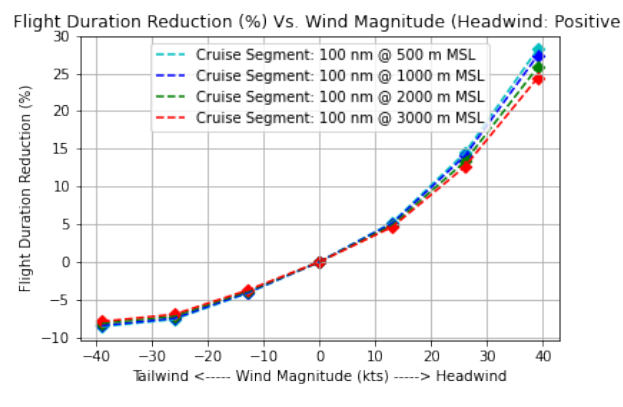


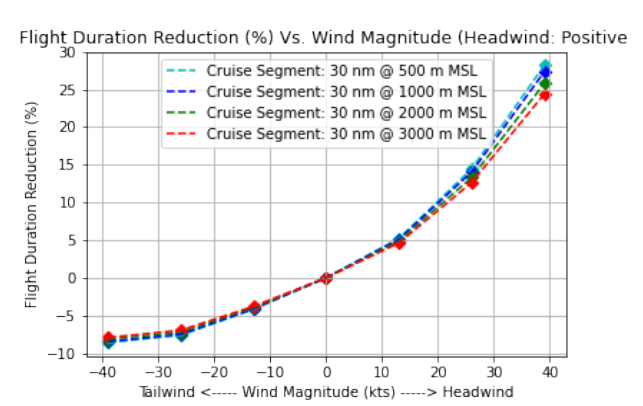
(a) Comparison of energy consumption for 100 nm cruise (b) Comparison of energy consumption for 30 nm cruise segment





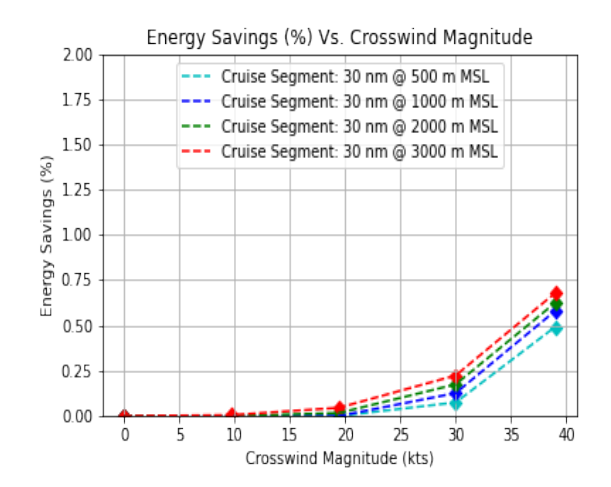
(c) Energy savings in percentage flying wind-optimal airspeed vs best-range airspeed for 100 nm cruise segment vs best-range airspeed for 30 nm cruise segment

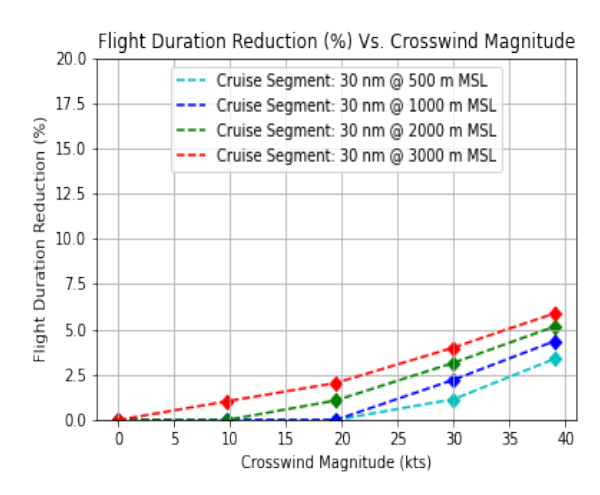




(e) Flight duration savings in percentage flying wind-optimal airspeed vs best-range airspeed for 100 nm cruise segment airspeed vs best-range airspeed for 30 nm cruise segment

Fig. 6 Energy consumption and flight duration results comparing wind-optimal airspeed with best-range airspeed under different headwind and tailwind conditions





- cruise segment
- (a) Comparison of energy savings in percentage for 30 nm (b) Comparison of flight duration savings in percentage for 30 nm cruise segment

Fig. 7 Energy consumption and flight duration results comparing wind-optimal airspeed with best-range airspeed under different crosswind conditions

# VI. Wind Magnitude Uncertainty

In the high-density and high-tempo, mature UAM airspace environments [5], one way to achieve a controlled UAM traffic flow to the vertiport could be by assigning time constraints at selected waypoints (metering fixes) that multirotor aircraft must meet using an onboard control system for dynamic airspeed adjustment [17]. This procedure is often characterized as the required time of arrival (RTA) [4]. Similarly, to maintain the minimum spatial separation between flights on two separate segments crossing a common waypoint or merging at a waypoint at the same altitude under high traffic density, the flights may be required to sequence the waypoint at a precise time (RTA) [18]. This research assumes that a scheduler would assign the required time of arrival (RTA) at the metering fix pre-departure based on desired cruise airspeed mode (wind-optimal or best-range) and wind forecast. Hence, the multirotor aircraft would adjust the airspeed in real-time based on the actual wind conditions to achieve the assigned RTA. To study the impact of wind magnitude uncertainty on the energy consumption by the multirotor aircraft while flying to meet the required time of arrival (RTA) assigned by a scheduler, wind conditions and distance to the metering fix are varied.

The different wind conditions involve varying wind magnitudes: [13 kts, 26 kts], and wind magnitude uncertainties: [-50 %, -30 %, -15 %, 0, 15 %, 30 %, 50 %]. The wind magnitude uncertainty is defined as:

Wind Magnitude Uncertainty = 
$$\frac{\text{Actual Wind Magnitude} - \text{Predicted Wind Magnitude}}{\text{Predicted Wind Magnitude}} 100$$
 (17)

The wind direction is assumed to be headwind because, as shown in Figure 6, it was determined that wind-optimal airspeed results are most sensitive to headwind conditions. This case study has considered two metering fixes from the multirotor aircraft's position (top-of-climb), i.e., 30 nm and 100 nm in cruise phase at 500 m above MSL.

The blue bars in Figure 8 represent the difference in energy consumption between flying a free flight time, i.e., without an assigned RTA flight at wind-optimal airspeed based on actual wind conditions and flying to meet the RTA assigned (based on wind-optimal airspeed and predicted wind) under actual wind conditions as follows:

$$\Delta E_{\text{Blue Bar}} = \text{Energy}_{\text{RTA}} - \text{Energy}_{\text{Wind-Optimal}}$$
 (18)

The orange bars in Figure 8 represent the difference in energy consumption between flying a free final time, i.e., without an assigned RTA flight at best-range airspeed under actual wind conditions and flying to meet the RTA assigned (based on best-range airspeed and predicted wind) under actual wind conditions as follows:

$$\Delta E_{\text{Orange Bar}} = \text{Energy}_{\text{RTA}} - \text{Energy}_{\text{Best-Range}}$$
(19)

From Sub-figures of Figure 8, it can be seen that variations in lengths of blue bars are much smaller than variations in lengths of orange bars with a change in wind magnitude uncertainty. Therefore, Sub-figures of Figure 8 show that

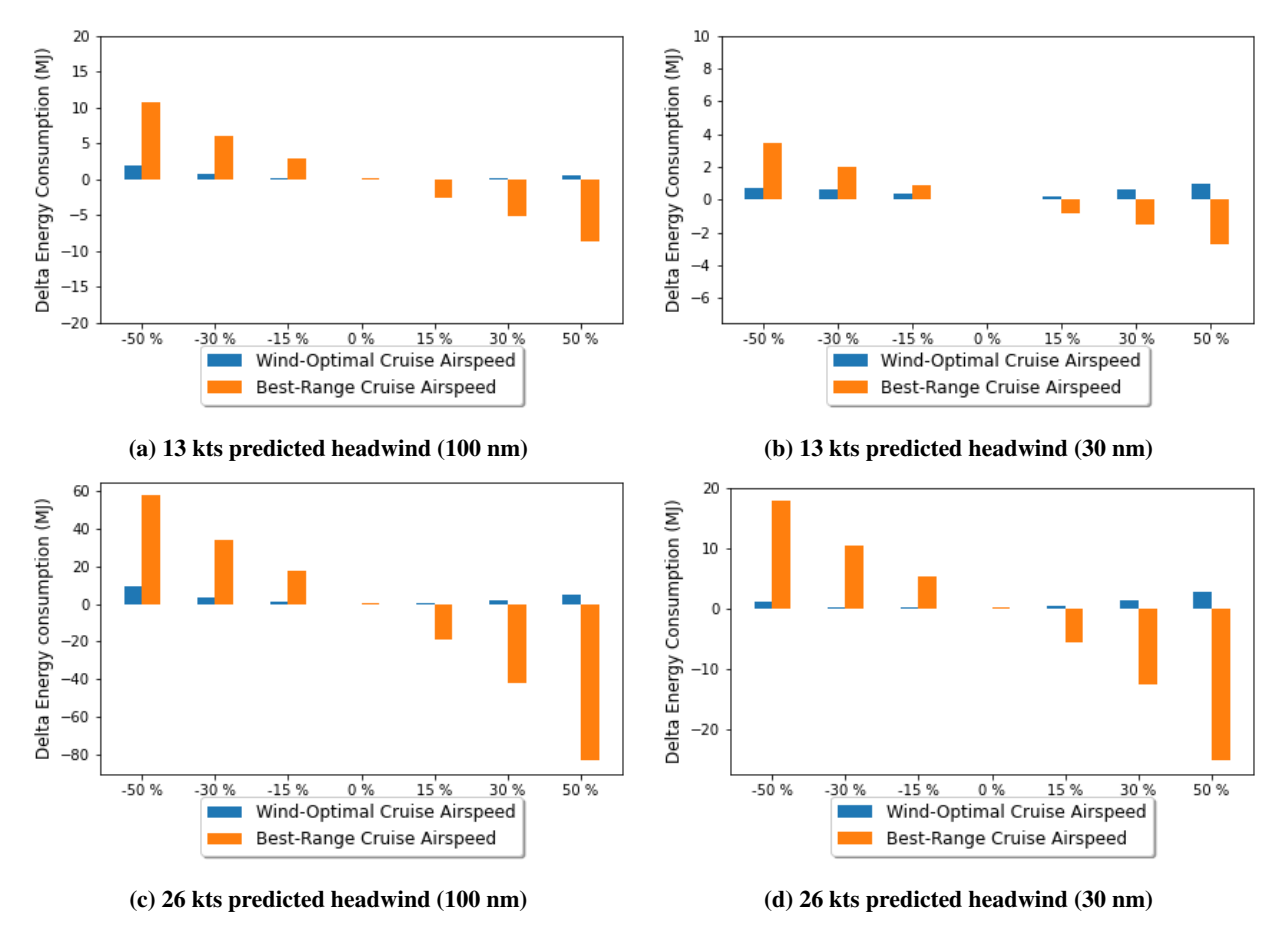


Fig. 8 Delta energy consumption while flying to meet an assigned RTA under various wind magnitude uncertainty for the best-range and wind-optimal cruise airspeed modes

flying at wind-optimal airspeed under wind magnitude uncertainty: i) has lower variability in energy consumption, and ii) provides higher predictability of energy consumption than flying at best-range airspeed. Hence, wind-optimal airspeed mode is better suited for UAM operations given low specific energy of current state-of-the-art Lithium-Ion Polymer (Li-Po) battery technology used for distributed electric propulsion (DEP) in multirotor aircraft [7, 19].

#### **VII. Conclusion**

This paper first investigates the effect of wind on the wind-optimal (minimum-energy) cruise airspeed for a NASA-proposed conceptual multirotor aircraft for the urban air mobility environment. Next, energy consumption and flight duration results are compared for flying at the wind-optimal airspeed mode and best-range airspeed mode on a great-circle cruise segment under different wind conditions. Finally, the difference in energy consumption when flying to meet the assigned required time of arrival based on actual wind conditions vs. predicted wind conditions are examined and compared for the two airspeed modes (wind-optimal and best-range) for different values of wind magnitude uncertainty.

In summary, the study shows the wind-optimal cruise airspeed is faster than the best-range airspeed under headwind conditions and slower than the best-range airspeed under tailwind conditions. The results show operational benefits of flying at the wind-optimal cruise airspeed compared to the best-range airspeed, especially in headwind conditions from both an energy consumption (0 - 7.5%) and flight duration (0 - 28%) perspective. On the other hand, there is only a slight operational benefit in energy consumption (0 - 2%) flying at the wind-optimal airspeed in tailwind conditions at the cost of a longer flight duration compared to flying at the best-range airspeed. The study also shows that flying at wind-optimal airspeed under wind magnitude uncertainty has lower variability and higher predictability of energy

# Acknowledgments

The authors thank Dr. Wayne Johnson, Christopher Silva, Dr. Robert Windhorst, and Dr. Jinhua Li from NASA Ames Research Center for discussions, reviews and helpful suggestions. The material is based upon work supported by NASA under award number NNA16BD14C for NASA Academic Mission Services (NAMS).

#### References

- [1] Johnson, W., Helicopter theory, Courier Corporation, 2012.
- [2] Slater, G., and Erzberger, H., "Optimal short-range trajectories for helicopters," *Journal of Guidance, Control, and Dynamics*, Vol. 7, No. 4, 1984, pp. 393–400.
- [3] Uber-Elevate, "Fast-forwarding to the future of on-demand, urban air transportation," https://www.uber.com/, 2019. [Online; accessed 19-June-2019].
- [4] Pradeep, P., and Wei, P., "Energy-efficient arrival with rta constraint for multirotor evtol in urban air mobility," *Journal of Aerospace Information Systems*, Vol. 16, No. 7, 2019, pp. 263–277.
- [5] Thipphavong, D. P., Apaza, R., Barmore, B., Battiste, V., Burian, B., Dao, Q., Feary, M., Go, S., Goodrich, H. J., Kenneth H, Idris, H. R., Kopardekar, P. H., Lachter, J. B., Neogi, N. A., Ng, H. K., Oseguera-Lohr, R. M., Patterson, M. D., and Verma, S. A., "Urban air mobility airspace integration concepts and considerations," 2018 Aviation Technology, Integration, and Operations Conference, 2018, p. 3676. doi:10.2514/6.2018-3676.
- [6] Bosson, C., and Lauderdale, T. A., "Simulation evaluations of an autonomous urban air mobility network management and separation service," 2018 Aviation Technology, Integration, and Operations Conference, 2018, p. 3365. doi:10.2514/6.2018-3365.
- [7] Johnson, W., "NDARC-NASA Design and Analysis of Rotorcraft," 2015.
- [8] Pradeep, P., Kulkarni, C. S., Chatterji, G. B., and Lauderdale, T. A., "Parametric Study of State-of-Charge for an Electric Aircraft in Urban Air Mobility," *AIAA AVIATION 2021 FORUM*, 2021.
- [9] Silva, C., Johnson, W. R., Solis, E., Patterson, M. D., and Antcliff, K. R., "VTOL Urban Air Mobility Concept Vehicles for Technology Development," 2018 Aviation Technology, Integration, and Operations Conference, 2018, p. 3847.
- [10] Pradeep, P., Lauderdale, T. A., Chatterji, G. B., Sheth, K., Lai, C. F., Sridhar, B., Edholm, K.-M., and Erzberger, H., "Wind-Optimal Trajectories for Multirotor eVTOL Aircraft on UAM Missions," AIAA AVIATION 2020 FORUM, 2020, p. 3271.
- [11] Yomchinda, T., Horn, J., and Langelaan, J., "Flight path planning for descent-phase helicopter autorotation," *AIAA Guidance, Navigation, and Control Conference*, 2011, p. 6601.
- [12] Tsuchiya, T., Ishii, H., Uchida, J., Ikaida, H., Gomi, H., Matayoshi, N., and Okuno, Y., "Flight trajectory optimization to minimize ground noise in helicopter landing approach," *Journal of guidance, control, and dynamics*, Vol. 32, No. 2, 2009, pp. 605–615.
- [13] Johnson, W., "Helicopter optimal descent and landing after power loss," 1977.
- [14] Becerra, V. M., "Solving complex optimal control problems at no cost with PSOPT," 2010 IEEE International Symposium on Computer-Aided Control System Design, 2010, pp. 1391–1396. doi:10.1109/CACSD.2010.5612676.
- [15] "Interagency Helicopter Operations Guide,", Jun 2016. URL http://forestry.alaska.gov/Assets/pdfs/aviation/ InteragencyHelicopterOperationsGuide(2016).pdf, [Online; accessed 31-April-2021].
- [16] Hale, F. J., and Steiger, A. R., "Effects of Wind on Aircraft Cruise Performance," *Journal of Aircraft*, Vol. 16, No. 6, 1979, pp. 382–387. doi:10.2514/3.58535, URL https://doi.org/10.2514/3.58535.
- [17] Michael K. DeJonge, M., Kentwood, "Required time of arrival (RTA) control system,", U.S. Patent 5121325A, June. 1992.
- [18] Lauderdale, T. A., Pradeep, P., Edholm, K.-M., and Bosson, C. S., "Separation at Crossing Waypoints Under Wind Uncertainty in Urban Air Mobility," AIAA AVIATION 2021 FORUM, 2021. doi:10.2514/6.2021-2351, URL https://arc.aiaa.org/doi/abs/10.2514/6.2021-2351.
- [19] Daigle, M., and Kulkarni, C., "Electrochemistry-based Battery Modeling for Prognostics," *Annual Conference of the Prognostics and Health Management Society* 2013, 2013, pp. 249–261.